ARTICLES

Characterization of the Tetratricopeptide-Containing Domain of BUB1, BUBR1, and PP5 Proves That Domain Amphiphilicity over Amino Acid Sequence Specificity Governs Protein Adsorption and Interfacial Activity

Sylvie Beaufils,[†] J. Günter Grossmann,[‡] Anne Renault,[†] and Victor M. Bolanos-Garcia*[,§]

Department of Biochemistry, University of Cambridge, Cambridge, U.K., Molecular Biophysics Group, Science and Technology Facilities Council, Daresbury Laboratory, Daresbury Science and Innovation Campus, Warrington, Cheshire, U.K., and Groupe Matiere Condensee et Materiaux, Universite de Rennes 1, Campus de Beaulieu, Rennes cedex, France

Received: November 27, 2007; Revised Manuscript Received: April 10, 2008

The tetratricopeptide motif repeat (TPR) is an α-helix-turn-α-helix motif that typically mediates protein−protein and, in some cases, protein−lipid interactions. Because of its success, this motif has been preserved through evolution and can be identified in proteins of a wide range of functions in lower and higher organisms. The N-terminal region of BUB1, BUBR1, and protein phosphatase 5 (PP5) contains tandem arrangements of the TPR motif. BUB1 and BUBR1 are conserved multidomain protein kinases that play a key role in the mitotic checkpoint, the mechanism that ensures the synchrony of chromosome segregation. PP5 is an enzyme that targets a wide range of protein substrates including single transmembrane receptors and mammalian cryptochromes. The N-terminal TPR domain of PP5 regulates the activity of the C-terminal catalytic domain through direct interaction with protein and lipid molecules. We portray the biophysical and biochemical properties of the tandem arrangements of the TPR motif of BUB1, BUBR1, and PP5 using far-UV spectroscopy, solution X-ray scattering, null ellipsometry, surface rheology measurements, and Brewster angle microscopy (BAM) observations. We show that, despite the low amino acid sequence conservation and different function, the TPR motif repeats of the three proteins exhibit similar interfacial properties including adsorption kinetics, high surface activity, and the formation of stable, rigid films at the air/water interface. Our studies demonstrate that domain amphiphilicity is of higher importance than amino acid sequence specificity in the determination of protein adsorption and interfacial activity.

1. Introduction

BUB1 and BUBR1 (BUB, budding uninhibited by benzimidazole) are essential components of the mitotic checkpoint, the mechanism that monitors the proper assembly of the mitotic spindle and blocks the onset of anaphase until all chromosomes are stably attached to kinetochores. BUB1 and BUBR1 are highly conserved in eukaryotes and organized in three domains: an N-terminal domain that contains tandem arrangements of the tetratricopeptide motif repeat (TPR), a middle region of low structural complexity and a catalytic serine/threonine kinase C-terminal domain.[1] BUB1 acts as an upstream component of the mitotic checkpoint pathway, while BUBR1 is a downstream component that inhibits the regulatory protein CDC20. BUB1 exhibits asymmetry in prometaphase cells, and its immunodepletion abolishes the binding of CENP-E, Mad1, Mad2, BUBR1, and BUB3 to the kinetochore, suggesting that BUB1 binds closer to the core of the kinetochore than these proteins.[2] The characterization of mutants of BUB1 from *S. pombe* has shown that residues located in the N-terminal TPR-motif-containing region are crucial for several functions such as kinetochore accumulation of BUB1 in checkpoint-activated cells, cell cycle arrest induced by spindle assembly checkpoint activation, recruitment of BUB3 and Mad3 to kinetochores in checkpoint-activated cells, and nuclear accumulation of BUB1, BUB3, and Mad3 in cycling cells.[3] Protein phosphatase 5 (PP5) is a monomeric enzyme that consists of two domains: an N-terminal domain that is organized as a triple tandem arrangement of the tetratricopeptide (TPR) motif and a C-terminal phosphatase domain. The TPR domain of PP5 regulates the activity of the C-terminal catalytic domain in a process that requires the physical contact of the TPR units with arachidonic acid (AA).[4] The canonical TPR is a degenerate tandem repeat of 34 amino acid residues encoding an α-helix-turn-α-helix motif that was first identified in cell cycle division proteins.[5] This motif has now been recognized in a wide range of proteins of diverse biological functions such as cell cycle regulation, transcription control, neurogenesis, protein kinase inhibition, mitochondrial and peroxisomal protein transport, Rac mediated activation of NADPH oxidase, and protein folding.[6] The TPR is often present in tandem arrays of 3−16 units, although individual TPR units may be dispersed throughout the protein

* Corresponding author. Address: Department of Biochemistry, University of Cambridge, 80 Tennis Court Road, Cambridge CB2 1GA, U.K. Phone: 44-0-1223-766029. Fax: 44-0-1223-766002. E-mail: victor@cryst.bioc.cam.ac.uk.

[†] Universite de Rennes 1.

[‡] Daresbury Science and Innovation Campus.

[§] University of Cambridge.

10.1021/jp711222s CCC: $40.75
Published on Web 06/12/2008

sequence. The TPR typically mediates protein−protein interactions and is found in a wide range of organisms, ranging from bacteria to humans.[6] The crystal structure of various TPR motifs, including that of protein phosphatase 5 (PP5), shows that adjacent TPR units are packed together to form a regular series of antiparallel α-helices rotated relative to one another by a constant 24°. The uniform arrangement of neighboring α-helices gives rise to the formation of a regular, elongated amphipathic groove.[7] This topology constitutes a suitable platform for target proteins; in PP5, these include mammalian cryptochromes CRY1 and CRY2[8] and the single transmembrane atrial natriuretic peptide receptor.[9]

Given the amphipathic character that results from the spatial arrangement of tandem repeats of the TPR motif, we set out to characterize the interfacial properties of the TPR-containing domain of BUB1, BUBR1, and PP5. We present evidence that, despite their different functions, low amino acid sequence conservation, and oligomerization state in aqueous solutions, the TPR domains of the three proteins show striking similarity at air/water interfaces, which includes similar adsorption kinetics, surface activity, stability, and rheology. Taken together, our studies show the greater importance of overall protein amphiphilicity over the particular amino acid sequence in the determination of interfacial properties of tandem arrangements of the TPR motif.

2. Experimental Section

2.1. Cloning, Expression, and Purification. The gene region encoding the N-terminal domain of yeast BUB1 residues 1−230 was extended using conventional PCR and cloned in frame downstream of the *gst* gene. The identity of the resulting expression vector, pGST-BUB1p(1−230), was confirmed by DNA sequencing. *E. coli* BL21 (DE3) cells were transformed with this plasmid using a conventional heat-shock protocol. Protein expression was carried out as follows: when the $O.D._{600\,nm}$ value of the bacterial culture grown at 37 °C was 0.6−0.7, cells were induced with IPTG and harvested 3 h after induction. The cell pellet was resuspended in TBS buffer (0.02 M Tris, 0.1 M NaCl, pH 8.0) containing a cocktail of protease inhibitors. Cells were lysed in TBS buffer containing Bugbuster (Novagen Inc., U.K.). After centrifugation at 18 000 rpm for 45 min at 4 °C, the soluble fraction was loaded onto an XK 26 column packed with glutathione−sepharose resin previously equilibrated in TBS buffer solution. After washing with approximately 20 volumes of TBS, the GST tag was cleaved and removed using a second sepharose−glutathione column. The N-terminal domain of human BUBR1, residues 1−204, was expressed in *E. coli* as a GST fusion. Protein expression and purification was carried out according to the protocol described above. The tetratricopeptide motif repeat of human protein phosphatase 5, residues 16−181 (PP5(16−181)), containing a six-histidine tag at the N-terminal region was expressed in *E. coli* BL21 Codon plus and purified by Ni-NTA affinity followed by size-exclusion chromatography according to conventional protocols. The identity of recombinant BUB1p(1−230), BUBR1(1−204), and PP5(16−181) was confirmed by MALDI-TOF, N-terminal sequencing by the Edman degradation method, and amino acid composition analysis at the PNAC facility (Department of Biochemistry, University of Cambridge). Buffer solutions of identical composition were used for the purification and concentration of each protein domain. Analytical and preparative size-exclusion chromatography was performed in a HiLoad 26/60 Superdex 75 preparative grade column previously equilibrated in TBS buffer. For analytical size-exclusion chromatography, the following proteins were used as molecular mass standards: BSA (67 kDa), ovalbumin (43 kDa), chymotrypsinogen A (25 kDa), and ribonuclase A (13 kDa).

2.2. Circular Dichroism. Far-UV circular dichroism spectra were recorded on an AVIV 62-S spectropolarimeter (AVIV, Lakewood, NJ) previously calibrated with camphorosulfonic acid and equipped with a temperature control unit. In all experiments, spectra were recorded at 20 °C in a 0.1 cm quartz cell using an average time of 0.5 s, a step size of 0.5 nm, and a 1 nm bandwidth and averaged over 20 scans. The global α-helix content was calculated with the program CDPro[10] and from the molar residue ellipticity at 222 nm, according to a method previously reported.[11] The dependence of CD signal on protein concentration was calculated by triplicate using independent samples of concentrations ranging between 50 and 600 μg/mL (i.e., ≈2−22 μM). After subtraction of the buffer baseline, the CD data were normalized and reported as molar residue ellipticity. For studies of protein stability as a function of pH, protein solutions were prepared in 0.05 M sodium acetate, pH 4 and 5; 0.05 M sodium phosphate buffer, pH 6, 7, and 8; and 0.05 M sodium borate, pH 9 and 10. The concentration of protein solutions was determined from amino acid composition analysis at the PNAC facility (Department of Biochemistry, University of Cambridge). Far-UV CD analysis of all proteins was carried out immediately after gel filtration chromatography. For fatty acid binding experiments, the far-UV CD signal was recorded in the range from 260 to 180 nm in the presence of 50, 100, and 250 μM arachidonic acid.

2.3. Solution X-ray Scattering. High and low angle scattering data were collected at Station 2.1, Synchrotron Radiation Source, Daresbury Laboratory U.K., using a two-dimensional multiwire proportional counter at sample-to-detector distances of 1 and 4.25 m and an X-ray wavelength of 1.54 Å with beam currents between 120 and 200 mA. Each sample was exposed for 25 min in 30 s frames. Frames at the beginning and the end of each data collection were compared to exclude the possibility of protein aggregation and/or radiation damage. The data reduction involved radial integration, normalization of the one-dimensional data to the intensity of the transmitted beam, correction for detector artifacts, and subtraction of buffer scattering (OTOKO, SRS, Daresbury). The q range was calibrated with an oriented specimen of wet rat tail collagen (diffraction spacing 670 Å) and silver behenate (diffraction spacing 58.38 Å). BUB1p(1−230) solutions at concentrations ranging between 1 and 10 mg/mL (i.e., 146−365 μM) were prepared in TBS buffer (pH 8.0) and analyzed at 20 °C. The profiles collected at both camera lengths were merged so as to cover the momentum transfer interval $0.03\ Å^{-1} < q < 0.77\ Å^{-1}$. The modulus of the momentum transfer is defined as $q = 4\pi \sin \Theta$, where 2Θ is the scattering angle and λ is the wavelength used. The maximum scattering angle corresponds to a nominal Bragg resolution of approximately 8 Å. The forward scattering intensity, radius of gyration (R_g), maximum particle dimension (D_{max}), and intraparticle distance distribution function [$p(r)$] were calculated from the scattering data using the indirect Fourier transform method program GNOM.[12] For determination of protein oligomerization state, the following proteins were used as references: BSA (67 kDa), ovalbumin (43 kDa), and thaumatin I (22 kDa). All samples were prepared in TBS buffer. Reconstruction of the molecular shape of the TPR domain of dimeric BUB1 from the scattering profile alone was carried out using the *ab initio* program Gasbor.[13] Numerous independent shape restorations were performed using both no symmetry as well as 2-fold symmetry constraints. Only the latter

provided highly consistent shape models that are reminiscent of the characteristic particle shape observed in the crystal structure of several TPR domains of diverse proteins, including that of human protein phosphatase 5 (PDB entry 1A17 and 1WAO),[7] new lipoprotein 1 from *E. coli* (Npl-1) (PDB entry 1XNF),[14] and TPR2A of human HOP (PDB entry 1ELR).[15] To check the results of *ab initio* modeling, the program DAMMIN (www.embl-hamburg.de/ExternalInfo/Research/Sax/dammin.html) was also used. These models were similar to those obtained with GASBOR but at a lower resolution due to the algorithm employed which uses a smaller number of atoms at larger, regularly spaced distances. Because the crystal structure of the TPR motif of protein phosphatase 5 (PDB entry 1WAO) corresponds to the top hit of fold recognition analyses of the N-terminal region of BUB1/BUBR1 proteins,[16] it was superimposed onto the low resolution structure of BUB1p(1−230) and visualized using the program Pymol.[17]

2.4. Null Ellipsometry and Surface Pressure Measurements. Interfacial layers were prepared on a circular trough ($S = 20$ cm^2), and the surface pressure was measured with a sensor (Nima Technology Ltd., England) using a Wilhelmy plate with a precision of ±0.5 mN/m. The ellipsometric measurements were carried out with a house-made ellipsometer[18] operated with a He−Ne laser ($\lambda = 632.8$ nm, Melles Griot) polarized with a Glan-Thompson polarizer at 18 °C. The incidence angle of the light on the surface was 1° away from the Brewster angle. After reflection on the water surface, the laser light passed through a $\lambda/4$ retardation plate, a Glan-Thompson analyzer, and a photomultiplier. Through a computer-controlled feedback loop, the analyzer automatically rotated toward the extinction position. In this "null ellipsometer" configuration,[19] the analyzer angle, multiplied by 2, yielded the value of the ellipsometric angle (Δ), i.e., the phase difference between parallel and perpendicular polarization of the reflected light. The precision on Δ is ±0.5°. The laser beam probed a surface of 1 mm^2 and a depth in the order of 1 μm. In the case of amphiphilic molecules, there is an excess concentration of molecules adsorbed at the interface (presumably due to a change in the chemical potential near the surface) compared to that in the bulk. Consequently, the ellipsometric angle (Δ) is mainly sensitive to the interfacial layer and is proportional to the quantity of proteins adsorbed at the interface. Hence, the variation of the ellipsometric angle is a relevant probe for changes occurring at the interface. Using the measured ellipsometric angle (Δ) and estimating the refractive index increment of the protein to 0.2 mL/g, the surface concentration (Γ) of adsorbed protein was calculated using the relationship between Δ and Γ reported by De Feijter and Benjamins: Γ (mg/m^2) = 0.2Δ (°).[20] Initial values of the ellipsometric angle (Δ_0) and surface tension of pure buffer solutions were recorded on the subphase for at least half an hour. These values have been subtracted from all data presented below. Values of Δ and surface pressure (π) were stable and recorded every 4 s with a precision of ±0.5° and ±0.5 mN/m, respectively, at 20 °C. Protein solutions were prepared in the range 1−80 μg/mL (i.e., ≈ 36 nM−3 μM) in 0.02 M sodium phosphate buffer (pH 7) for null ellipsometry, surface pressure, and surface rheology measurements as well as Brewster angle microscopy (BAM) observations.

2.5. Determination of the Shear Elastic Constant. The principles and implementation of our experimental setup for the measurement of the lateral rigidity of interfacial layers and the procedure for data analysis have been extensively described before.[21] Briefly, at the center of a 48-mm-diameter Teflon trough, a 10-mm-diameter paraffin-coated aluminum disk floats at the air/water interface, in contact with the interfacial layer, whose rigidity is measured. The subphase is 5 mm deep. The float carries a small magnet and is kept centered by a permanent magnetic field, $B_0 = 6 \times 10^{-5}$ T, parallel to the Earth's field and created by a small solenoid located just above the float. Sensitive angular detection of the float rotation is achieved by using a mirror fixed on the magnet to reflect a laser beam onto a differential photodiode. A sinusoidal torque excitation is applied to the float in the 0.01−100 Hz frequency range by an oscillating field perpendicular to the permanent solenoid field. The latter field acts as a restoring torque equivalent to an interfacial layer with a rigidity of 0.16 mN/m. This number set the sensitivity limit of the rheometer. The device behaves like a simple harmonic oscillator. The resistance that the interfacial layer opposes to the rotation of the float is directly measured. An important advantage of this setup is the absence of a physical link between the outside and the float torsion (i.e., no torsion wire). This allows high sensitivities such that the applied deformation is very small, below $\mathbf{u}_{xy} \sim 10^{-7}$, where $\mathbf{u}_{xy}$ corresponds to the deformation tensor. This device introduces very small excitation strains (from 10^{-3} down to 10^{-6}) to the system. Because in previous experiments we have shown that pure shear elastic response spectra exhibit a linear stress−strain relationship over this range,[21] we concluded that the rotation coupling between the float and the contacting interfacial layer is satisfactory. Moreover, we have showed that such small strains do not create plastic deformations on fragile surface objects.[22] For the experimental procedure, the amplitude and phase of the mechanical response of the pure subphase was first analyzed in the frequency range 0.01−100 Hz to assess that no rigidity was detected. This measurement takes approximately 1 h. Then, the protein solution was directly poured in the trough and the mechanical response of the layer formed at the interface recorded at a fixed frequency of 5 Hz. At the end of the kinetics, when the shear elastic constant (μ) (expressed in mN/m) reached a constant value, a new measurement between 0.01 and 100 Hz was recorded to determine whether the system behaves as an elastic layer. Rigidity measurements were carried out in parallel to ellipsometry. All of the experiments were performed at 18 °C.

3. Results and Discussion

3.1. BUB1p(1−230), BUBR1(1−204), and PP5(16−181) Are Stable Domains. Since the TPR units of PP5 show local structure similarity with the N-terminal region of BUB1 and BUBR1,[16] we aimed to determine the stability and interfacial properties of yeast BUB1, residues 1−230; human BUBR1, residues 1−204; and PP5, residues 16−181. Far-UV CD spectroscopy showed that BUB1p(1−230) is an all-α-helix domain stable in the pH range 6−9 (Figure 1A), a stability profile that is very similar to that of human BUBR1(1−204).[16] In contrast, far-UV CD spectra recorded at the same concentrations (50−200 μg/mL) and pH 5 provided inconsistent ellipticity values because a slow but continuous protein precipitation was observed. This behavior was somewhat expected because of the predicted isoelectric point of this domain (pI 5.08). At pH lower than 5, a predominantly disordered structure was observed (Figure 1A). The thermal stability of the three TPR domains was also investigated by far-UV CD. A detailed account of the kinetics of thermal unfolding of these TPR domains will be published elsewhere. Briefly, the three TPR domains undergo a cooperative two-state thermal unfolding transition, being that of PP5(16−181) less cooperative than that of BUB1p(1−230) and human BUBR1(1−204). The ΔH value of thermal denaturation of these domains is within the range 43−52 kcal/mol,

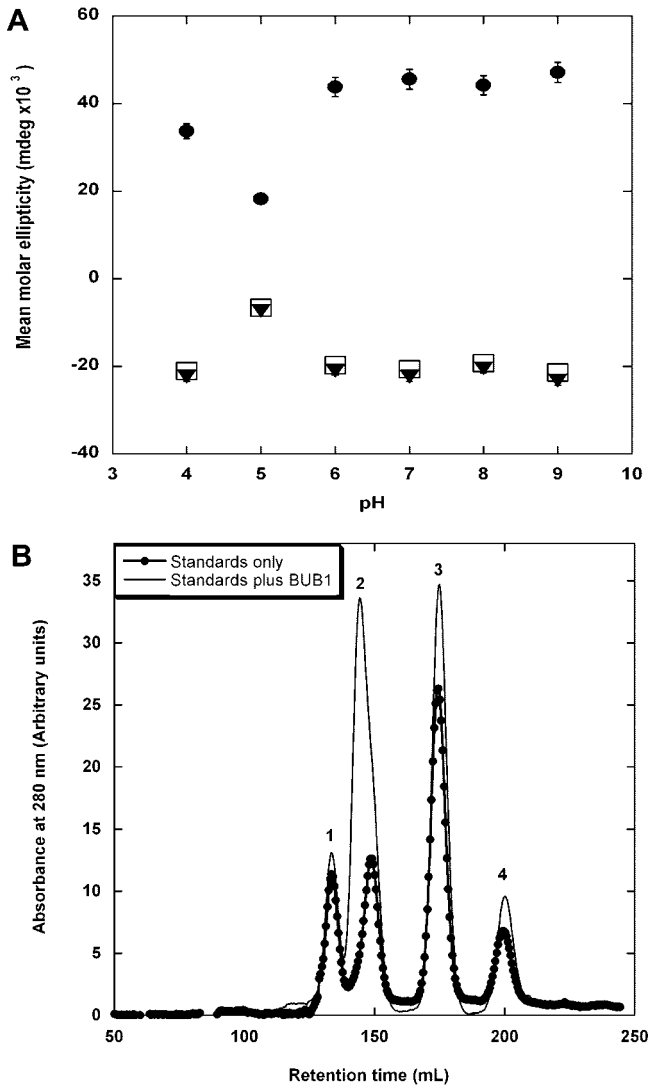

Figure 1. CD spectroscopy and gel filtration analysis. Far-UV CD spectroscopy and analytical size-exclusion chromatography of BUB1p(1−230). (A) Mean molar ellipticity recorded at 190 nm (●), 208 nm (▼), and 222 nm (□). The protein concentration was 600 μg/mL (i.e., ≈22 μM). (B) Size-exclusion chromatogram of molecular weight markers only (●): peak 1, bovine serum albumin; peak 2, ovalbumin; peak 3, chymotrypsinogen A; peak 4, ribonuclease A. For the second chromatogram (—), the same molecular weight markers were combined with BUB1p(1−230) prior to gel filtration. This experiment shows that the N-terminal domain of BUB1 forms stable dimers but not oligomers of higher order, as it was detected only in the fractions containing ovalbumin (MW 43 kDa).

which is similar to that observed in other tandem arrangements of the TPR motif of similar size and aggregation state (i.e., 40−65 kcal/mol).[23,24] The comparison of the apparent melting temperatures (T_m) of PP5(16−181), BUBR1(1−204), and BUB1p(1−230) indicates that thermal stability increases as follows: PP5(16−181) < BUBR1(1−204) < BUB1p(1−230), with a T_m value of 48, 51, and 62 °C, respectively (Table 1).

3.2. TPR Domains Show Similar Topology but Different Oligomerization States. In a previous report, we showed that PP5(16−181) and BUBR1(1−204) are organized as monomers and as a mixture of dimers and tetramers, respectively.[16] Now, we present evidence that BUB1p(1−230) self-associates to forms dimers. No oligomers of higher complexity were detected with this method (Figure 1B). Small angle X-ray scattering (SAXS) and nano-ES mass spectrometry confirmed that BUB1p(1−230) is predominantly dimeric in aqueous solutions

TABLE 1: Apparent Melting Temperatures (T_m) and Mean Molar Ellipticity of TPR Domains Derived from Far-UV CD Data

protein domain	T_m (°C)	mean molar residue ellipticity at 222 nm
BUB1p(1−230)	62	−20 600
BUBR1(1−204)	51	−19 200
TPR-PP5(16−181)	48	−19 700

(data not shown). SAXS provides low resolution structural data that allows for the calculation of the mean particle size (radius of gyration, R_g) and the maximum intramolecular distance (D_{max}). These two parameters give information on the compactness of the molecule and the maximum extension reached by the molecule in solution. The maximum intramolecular distance of BUB1p(1−230) in the concentration range 10−15 mg/mL (≈360−540 μM) indicates that this domain adopts an elongated conformation (D_{max} = 100 Å) (Figure 2A and B). Moreover, the value of the radius of gyration (30.4 ± 0.2 Å) was similar to that estimated from the crystal structure of PP5 residues 19−178 (≈33 Å) (Figure 2C). Superposition of the crystal structure of the latter on the shape of dimeric BUB1p(1−230) derived from SAXS data evidences the high local topology similarity of these domains (Figure 2A). Because the crystal structure of TPR-PP5 (PDB entry 1A17) corresponds to a dimeric protein that is significantly smaller (≈160 residues/chain) than that of BUB1p(1−230), Figure 2A shows that the edge regions of the reconstructed shape of BUB1p(1−230) are not occupied by the structure of TPR-PP5.

3.3. BUB1p(1−230), BUBR1(1−204), and PP5(16−181) Are Stable at Air/Water Interfaces. We next asked how similar these proteins would behave when adsorbed at the air/water interface. The N-terminal TPR domains of BUB1, BUBR1, and PP5 share low amino acid residue conservation: 21% of identity between yeast BUB1 and human BUBR1, 6% between yeast BUB1 and human PP5, and 3% between human BUBR1 and human PP5 (Figure 3). However, in the three proteins, the tandem arrangement of TPR units defines a continuous amphipathic groove.[7] Because it has been proposed that, in all-α-helix proteins that contain tandem repeats of amphipathic α-helices the affinity of the protein for water/air interfaces is related to the magnitude of the hydrophobic moment (μH),[25] we set out to calculate this parameter for the three TPR domains. μH (which is usually expressed in kcal/mol) of the 11 putative α-helices of BUB1p(1−230) was as follows: α-helix 1 (10−23), 0.25; α-helix 2 (29−50), 0.24; α-helix 3 (56−72), 0.23; α-helix 4 (81−97), 0.41; α-helix 5 (104−119), 0.35; α-helix 6 (122−137), 0.41; α-helix 7 (142−156), 0.36; α-helix 8 (158−172), 0.64; α-helix 9 (176−194), 0.51; α-helix 10 (205−215), 0.34; α-helix 11 (220−229), 0.43 kcal/mol. The average hydrophobic moment (μH_{avg}) of BUB1p(1−230) (i.e., $\mu H_{avg} = \Sigma \mu H$/number of amphipathic α-helices) was 0.38 kcal/mol per residue, which is slightly higher than that of human BUBR1(1−204) (μH_{avg} = 0.32 kcal/mol per residue) and PP5(16−181) (μH_{avg} = 0.36 kcal/mol per residue). The calculated μH_{avg} value of the three TPR domains was lower than that of apoC-I (μH_{avg} = 0.45 kcal/mol per residue)[26] and apoA-II (μH_{avg} = 0.41 kcal/mol per residue),[27] which are proteins constituted by two amphipathic α-helix repeats connected by a short loop region[28] that exhibit high surface activity.[29] Moreover, null ellipsometry measurements showed that, even though BUB1p(1−230), BUBR1(1−204), and PP5(16−181) exhibited a similar maximal surface pressure (i.e., between 18 and 20 mN/m) at the bulk concentration of 30 μg/mL (Figure 4A), BUB1p(1−230) presented a much lower

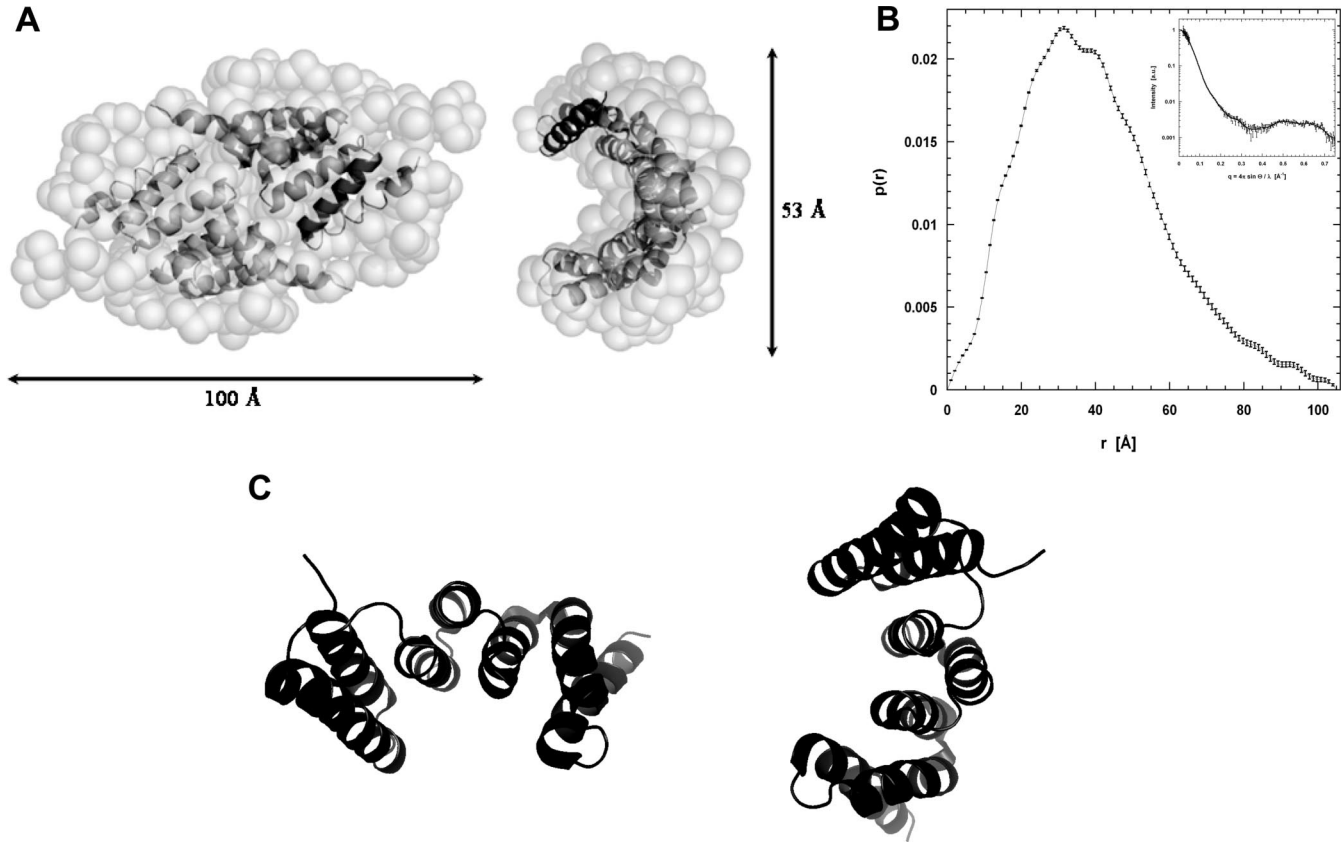

Figure 2. Small angle X-ray scattering. (A) Shape-reconstruction analysis of the BUB1p(1−230) dimer from SAXS data. (B) Distance distribution [$p(r)$] function of BUB1p(1−230). Inset, SAXS scattering profile showing that the overall conformation of the BUB1p(1−230) dimer is well preserved in aqueous solution. (C) Topology of the TPR domain of PP5. Left, the ribbon diagram shows that the domain consists of a triple repeat of the TPR motif. The amphipathic groove is defined by the concave face of this domain (α-helices 1, 3, 5, and 7). Right, the side view of the triple TPR repeat motif shows that it forms a right-handed superhelical structure. Figures generated with Pymol[17] from the Protein Data Bank (PDB entry 2BUG).

quantity of matter adsorbed at the interface than BUBR1(1−204) and PP5(16−181) (2.5, 4.0, and 4.7 mg/m^2, respectively) (Figure 4B). As BUB1p(1−230), BUBR1(1−204), and PP5(16−181) do not have the same molecular mass (54, 47, and 38 kDa, respectively), a fairer comparison requires converting Γ from mg·m^{-2} to mol·m^{-2}. The Γ plateau value of BUB1p(1−230), BUBR1(1−204), and PP5(16−181) was 4.6×10^{-4}, 8.5×10^{-4}, and 12.3×10^{-4} mol·m^{-2}, respectively. Hence, it seems that BUB1p(1−230) is the most surface active of the three protein domains, since less matter and molecules were required to achieve a similar maximal surface pressure than BUBR1(1−204) and PP5(16−181). Consistent with null ellipsometry, Brewster angle microscopy (BAM), which is very sensitive to the amount of matter adsorbed at the interface, allowed the direct observation of the rapid migration of BUB1p(1−230) from the bulk toward the surface. For instance, at the low concentration of 1 μg/mL, protein adsorption could be noticed as early as 1 min after deposition (data not shown). After 10 h, the protein interfacial layer thus formed remained stable, showed a high contrast with respect to pure buffer solution, and was homogeneous at the micrometer scale (data not shown).

3.4. Adsorption Kinetics. The adsorbed surface concentration and surface pressure of BUB1p(1−230) and PP5(16−81) monitored at the low bulk concentration of 1 μg/mL (36 and 54 nM) (data not shown) made it possible to record initial adsorption events, which in turn allowed extraction of several parameters that are relevant to surface activity. Two of these parameters were obtained from the plot of Γ versus π (Figure 5). Γ_0 is the surface concentration at which the surface pressure becomes different from zero and is obtained from the intersect of the slope π vs Γ, as shown in Figure 5. The parameter θ, which was extracted from the slope of the Γ−π curve, corresponds to the increase of surface pressure relative to the increase of surface concentration.[30] In the first steps of adsorption of BUB1p(1−230) and PP5(16−181) at this low bulk concentration, the transport of protein molecules from the subphase to the interface was assumed to be a diffusion-controlled process. Therefore, the surface concentration (Γ) followed the relation of Ward and Tordai,[31] allowing the calculation of the diffusion coefficient (D) (i.e., the initial part of the $\Gamma - t^{1/2}$ plot exhibits a linear dependence). The magnitude of the diffusion coefficient of BUB1p(1−230) ($D = 0.7 \times 10^{-10}$ m^2·s^{-1}) was similar to that of globular proteins of a similar size[20] and of the same order of magnitude as that of BUBR1(1−204) ($D = 4.8 \times 10^{-10}$ m^2·s^{-1}) and PP5(16−181) ($D = 3 \times 10^{-10}$ m^2·s^{-1}). Figure 5 shows that the Γ_0 value of BUB1p(1−230) was significantly lower than that of PP5(16−181) and BUBR1(1−204) (i.e., 0.5 mg/m^2 against 0.9 and 1.1 mg/m^2, respectively) while θ increased in the following order: BUBR1(1−204), BUB1p(1−230), and PP5(16−181) (10, 12, and 16 mg·m/m^2, respectively). However, as the maximal surface pressure and magnitude of θ were lower than the values reported for other proteins,[32] it seems that BUBR1(1−204), BUB1p(1−204), and PP5(16−181) do not belong to the group of extremely surface active proteins.

It can be argued that the high surface activity simply reflects the unfolding of the domain at air/water interfaces, which will result in the full exposure and rapid adsorption of the hydro-

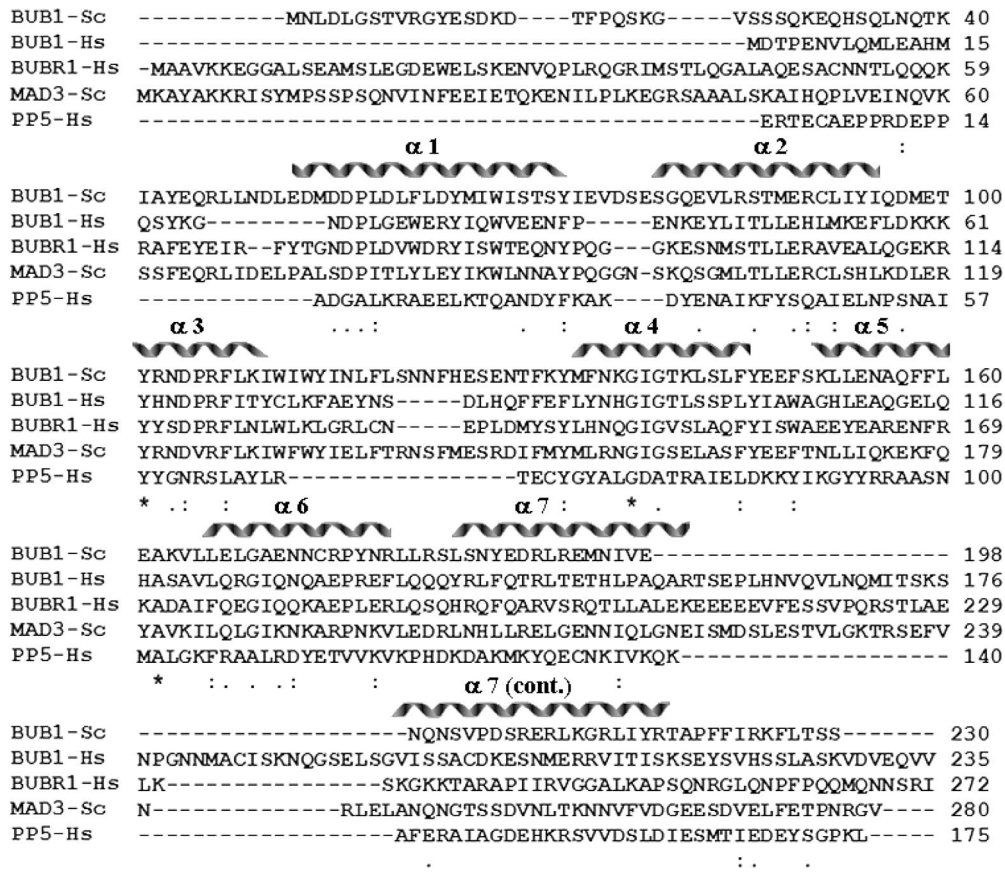

Figure 3. Sequence alignments. The alignments produced with CLUSTALW show that although the N-terminal domain of BUB1 and BUBR1 and PP5 present a triple tandem of the TPR motif, they share low amino acid residue conservation. The α-helices shown above the alignments correspond to those defined in the crystal structure of the TPR domain of PP5 (PDB entry 1A17).

phobic face of amphipathic α-helices at the interface. However, previous studies on monolayers of the TPR domain of human BUBR1 under native and denaturing conditions (i.e., pH 7 and 2, respectively) suggested this was not the case. BUBR1 remained at least partially folded at pH 7, while at pH 2 a much higher protein surface concentration, surface activity, and rigidity were noticed.[16] Besides, the behavior of BUBR1 as a function of pH revealed that, under conditions that promote protein unfolding, the amphipathic α-helices occupy more space and establish a more complex network of interactions at the interface.[16]

It is interesting to note that other proteins constituted by amphipathic α-helix-turn-α-helix repeats, such as the family of exchangeable apolipoproteins, exhibit different adsorption kinetics and maximal surface activity compared to the three TPR-containing proteins. The former protein family exhibits a different fold (i.e., they are organized as α-helix bundles), a feature that seems to account for the difference in the kinetics of adsorption and maximal interfacial activity. This notion is further supported by similar experiments conducted in full length proteins of different fold and secondary structure, including ovalbumin,[33] and protein domains such as PH and SH2 (Beaufils, S.; Renault A. Unpublished results). Besides, the study of monolayers of exchangeable apolipoproteins apoA-II, apoC-I, and apoC-III has revealed that the gradual compression of the protein monolayer promotes specific conformational changes at the air/water interface.[26,27] It would be important to establish whether a more complex fold, such as the TPR domain, can undergo similar conformational changes during lateral compression at air/water interfaces.

3.5. Evolution of the Shear Elastic Constant. The evolution of the shear elastic constant of BUB1p(1−230), BUBR1(1−204), and PP5(16−181) interfacial layers was measured at a fixed frequency of 5 Hz (Figure 6). At the end of each kinetics (around 12 h, indicated by the arrow in Figure 6), the amplitude and phase of the mechanical response of the interfacial layer was analyzed by estimation of the angular deviation [$\theta(\omega)$] in the frequency range 0.01−100 Hz. For BUB1p(1−230), BUBR1(1−204), and PP5(16−181), the real part and the imaginary part of the response were well adjusted with an elastic layer model (i.e., a simple harmonic oscillator), as shown in the inset of Figure 6 for BUB1p(1−230). Our experiments did not enable us to get a detailed description of the nonelastic part of the rheological response of the adsorbed layer. The main information obtained from our measurements is whether the response of the layer adjusts well to an elastic model: this is the case for the three proteins and indicates that medium- and long-range interactions play a major role in the cohesion of the layer. The evolution of the shear elastic constant (μ) measured at 5 Hz for the three fragments in the first 2 h showed a similar trend (Figure 6). Although after this time the absolute value of μ of BUBR1(1−204) was higher than that of PP5(16−181), the evolution of the shear elastic constant remained strikingly similar: μ increased at the same rate of 10 mN/m/h over at least 10 h. In contrast, the shear elastic constant of BUB1p(1−230) varied very slowly (i.e., 1 mN/m/h). This observation indicates that the organization of the BUB1p(1−230) interfacial layer practically remained unaltered once it was formed. On the contrary, BUBR1(1−204) showed a more extensive network of long-range interactions. This behavior can be explained

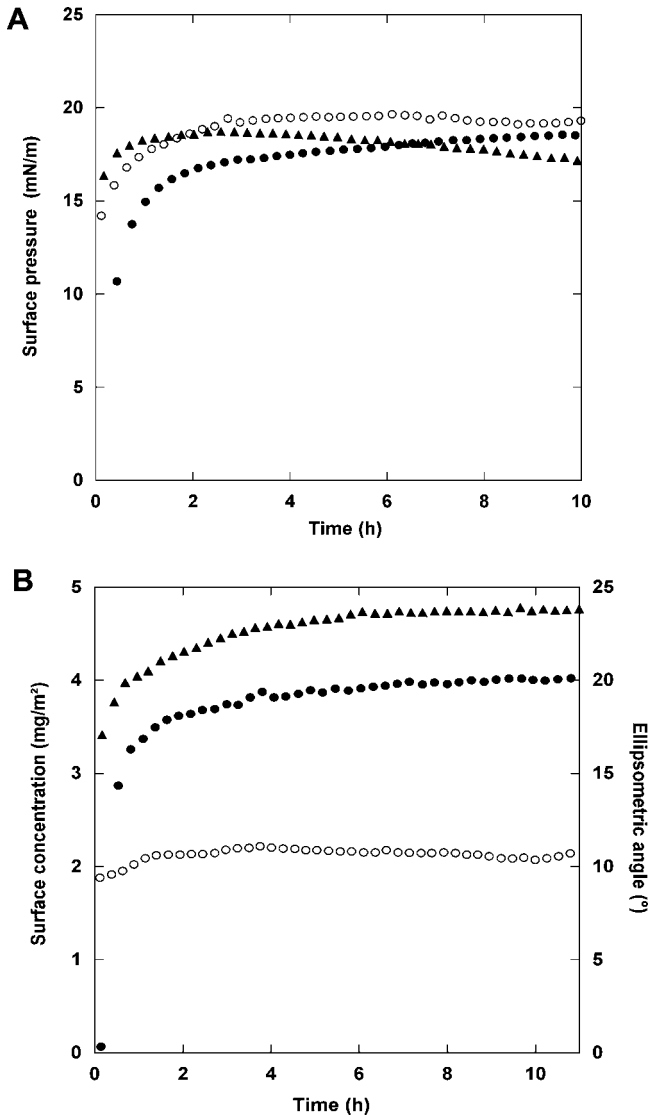

Figure 4. Interfacial properties of the TPR domain of BUB1, BUBR1, and PP5. (A) Surface pressure and (B) surface concentration ($\Gamma = 0.2\Delta$) together with the corresponding ellipsometric angle of BUB1p(1−230) at air/water interfaces determined by null ellipsometry measurements. Solutions of BUB1p(1−230) (○), BUBR1(1−204) (●), and PP5(16−181) (▲) were prepared at 30 μg/mL (1.0, 1.2, and 1.5 μM, respectively) in 20 mM phosphate buffer, pH 7.

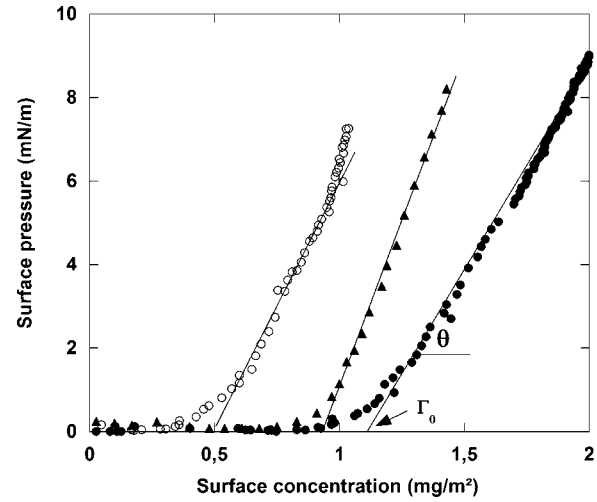

Figure 5. Surface pressure versus surface concentration of BUB1p(1−230), BUBR1(1−204), and PP5(16−181). θ corresponds to the slope $d\pi/d\Gamma$, and Γ_0 is the surface concentration at which the surface pressure becomes different from zero. Γ_0 is calculated from the intersect of the slope π vs Γ. BUB1p(1−230) (○), BUBR1(1−204) (●), and PP5(16−181) (▲) at 1 μg/mL (36, 54, and 42 nM, respectively) in 20 mM phosphate buffer, pH 7.

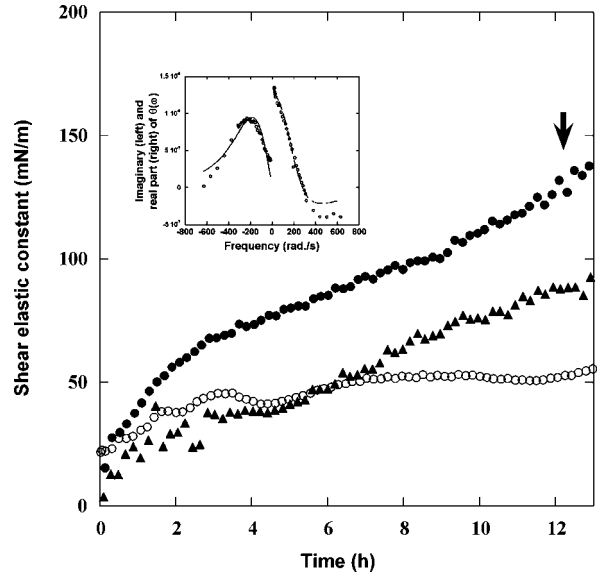

Figure 6. Rheology measurements of BUB1p(1−230), BUBR1(1−204), and PP5(16−181). The graph shows the evolution of the shear elastic constant (μ) versus time measured at a fixed frequency of 5 Hz, during protein adsorption at the interface. BUB1p(1−230) (○), BUBR1(1−204) (●), and PP5(16−181) (▲) at the bulk concentration of 30 μg/mL (1.0, 1.2, and 1.5 μM, respectively). The error bar on μ is ±5mN/m. Inset: at the end of the kinetics (around 12 h, indicated by the arrow in the graph), the angular deviation [$\theta(\omega)$] versus the pulsation was measured. The imaginary and real parts of the response fit an elastic layer model (harmonic oscillator). For clarity, the imaginary part has been plotted versus $-\omega$. The curves correspond to BUB1p(1−230) and are representative of BUBR1(1−204) and PP5(16−181).

considering that BUB1p(1−230) self-associates to form stable dimers at concentrations in the order 0.1−20 mg/mL (i.e., ≈3.6−730 μM) while human BUBR1(1−204) at similar concentrations exists as a mixed population of dimers, tetramers, and higher oligomerization states.[16] The latter condition allowed BUBR1(1−204) to establish various classes of contacts and rearrangements between protein molecules, giving place to the rapid formation of a polymer-like network. This stochastic process ultimately resulted in the formation of highly rigid interfacial layers. Overall, the magnitude of the shear elastic constant of BUB1p(1−230), BUBR1(1−204), and PP5(16−181) was of higher order of magnitude than that of other less surface active proteins.[32] The rigidity of the BUB1p(1−230), BUBR1(1−204), and PP5(16−181) interfacial layers indicates that these protein domains were stabilized at the interface by extensive medium-range and long-range interactions. This is consistent with the observation that extensive medium-range and long-range interactions are one important functional characteristic of the TPR motif[24] and constitute the interactions most frequently observed in all-α-helix proteins compared to the classes all-β, α+β, and α/β.[34]

3.6. Arachidonic Acid Binds Specifically to PP5(16−181). The binding of arachidonic acid (AA) to the TPR domain of PP5 contributes to the regulation of the phosphatase activity of this enzyme and protects the TPR domain from rapid proteolysis.[35] In contrast, the TPR-containing domain of the mitotic checkpoint protein BUBR1 does not bind arachidonic acid.[36] Despite this observation and the lack of evidence of the role (if

TABLE 2: Arachidonic Acid (AA) Titration of BUB1p(1-230) (Far-UV CD Data Were Recorded in the Range 260−180 nm at the Three Concentration Levels of AA Shown Below)

	mean molar residue ellipticity at		
arachidonic acid concentration (μM)	190 nm	208 nm	222 nm
0	43 532	−25 669	−25 250
50	43 690	−25 169	−25 033
100	45 190	−24 640	−24 838
200	42 800	−24 922	−24 910

any) of lipids in the mitotic checkpoint, we decided to establish whether the binding of AA to the TPR domain of PP5 is a property shared by BUB1p(1−230) given the high local structure similarity, μH_{avg}, and surface activity between these TPR domains. Far-UV CD spectroscopy showed that the addition of this fatty acid had no effect on the global secondary structure of BUB1p(1−230) (Table 2), confirming previous observations on the specificity of the interaction between the TPR domain of PP5 and AA.[35,36] Besides, the absence of lipid binding activity in BUB1p(1−230) is consistent with the lack of protection of this domain from limited proteolysis in the presence of AA (Bolanos-Garcia, V.M. Unpublished results).

4. Conclusions

It is well-established that the TPR motif typically mediates protein−protein interactions, and because of its success, it is widely distributed among species. We show that the N-terminal regions of BUB1, BUBR1, and PP5, all of which contain a tandem arrangement of the TPR motif and exhibit different thermal stabilities, are surface active domains. The latter property is relevant for the understanding of some of the functions of these proteins such as the mediation and/or stabilization of protein−protein and protein−lipid interactions, in the case of PP5, and protein−protein interactions in the case of BUB1 and BUBR1. To the best of our knowledge, this report is the first to present evidence that the overall amphiphilicity rather than the specific amino acid sequence determines the surface activity and rheology of tandem arrangements of the TPR motif at air/water interfaces. On a broader perspective, our study sheds light on the properties of repeat proteins when adsorbed at the air/water interface.

Abbreviations Used: BUB1, budding uninhibited by benzamidine protein 1; TPR, tetratricopeptide repeat; PP5, human protein phosphatase 5; far-UV CD, far-ultraviolet circular dichroism; O.D., optical density; Ni-NTA, nitrilotriacetic acid; GST, glutathione-S-transferase; BSA, bovine serum albumin; MWCO, molecular weight cutoff; PNAC, protein and nucleic acid chemistry; PDB, Protein Data Bank; MALDI-TOF, matrix-assisted laser desorption/ionization time-of-flight; CID, collision-induced dissociation; AA, arachidonic acid; BAM, Brewster angle microscopy; Dt, translational diffusion coefficient; SAXS, solution X-ray scattering.

Acknowledgment. We thank the Programme PICS (Projet International de Coopération Scientifique) CNRS for the financial support received (project propriétés interfaciales de protéines à motifs répétés). V.M.B.-G. acknowledges the support of Prof. Tom L. Blundell, Prof. A. Venkitaraman, and Cancer Research UK.

References and Notes

(1) Bolanos-Garcia, V. M. In *New Research on Signal Transduction*; Yanson, B. R. Ed.; Nova Science Publishers Inc: New York, 2007; p 1.
(2) Sharp-Baker, H.; Chen, R. H. *J. Cell Biol.* **2001**, *153*, 1239.
(3) Kadura, S.; He, X.; Vanoosthuyse, V.; Hardwick, K. G.; Sazer, S. *Mol. Biol. Cell* **2005**, *16*, 385.
(4) Kang, H.; Sayner, S. L.; Gross, K. L.; Russell, L. C.; Chinkers, M. *Biochemistry.* **2001**, *40*, 10485.
(5) King, R. W.; Peters, J. M.; Tugendreich, S.; Rolfe, M.; Hieter, P.; Kirschner, M. W. *Cell* **1995**, *81*, 279.
(6) Lamb, J. R.; Tugendreich, S.; Hieter, P. *Trends Biochem. Sci.* **1995**, *20*, 257.
(7) Das, K. A.; Cohen, P. T. W.; Barford, D. *EMBO J.* **1998**, *17*, 1192.
(8) Zhao, S.; Sancar, A. *Photochem. Photobiol.* **1997**, *66*, 727.
(9) Chinkers, M. *Proc. Natl. Acad. Sci. U.S.A.* **1994**, *91*, 11075.
(10) Sreerama, N.; Woody, R. W. *Anal. Biochem.* **2000**, *287*, 252.
(11) Bolanos-Garcia, V. M.; Soriano-Garcia, M.; Mas-Oliva, J. *Biochim. Biophys. Acta* **1998**, *1384*, 7.
(12) Svergun, D. I. *Appl. Crystallogr.* **1991**, *24*, 485.
(13) Svergun, D. I.; Pethoukov, M.; Koch, M. *Biophys. J.* **2001**, *80*, 2946.
(14) Wilson, C. G.; Kajander, T.; Regan, L. *FEBS J.* **2005**, *272*, 166.
(15) Scheufler, C.; Brinker, A.; Bourenkov, G.; Pegoraro, S.; Moroder, S.; Bartunik, L.; Hartl, H.; Moarefi, I. *Cell* **2000**, *101*, 199.
(16) Bolanos-Garcia, V. M.; Beaufils, S.; Renault, A.; Grossmann, J. G.; Brewerton, S.; Lee, M.; Venkitaraman, A.; Blundell, T. L. *Biophys. J.* **2005**, *89*, 2640.
(17) Delano, W. L. *Scientific D.*, San Carlos, CA, 2002.
(18) Berge, B.; Renault, A. *Europhys. Lett.* **1993**, *21*, 773.
(19) Azzam, R. M. A.; Bashara, N. M. *North Holland personal library*; Amsterdam, The Netherlands, 1977; p 340.
(20) De Feijter, J. A.; Benjamins, J.; Veer, F. A. *Biopolymers* **1978**, *17*, 1759.
(21) Venien-Bryan, C.; Lenne, P.-F.; Zakri, C.; Renault, A.; Brisson, A.; Legrand, J.-F.; Berge, B. *Biophys. J.* **1998**, *74*, 2649.
(22) Renault, A.; Lenne, P.-F.; Zakri, C.; Aradian, A.; Venien-Bryan, C.; Amblard, F. *Biophys. J.* **1999**, *76*, 1580.
(23) Cortajanera, L. A.; Regan, L. *Protein Sci.* **2006**, *15*, 1193.
(24) Beddoe, T.; Bushell, S. R.; Perugini, M. A.; Lithgow, T.; Mulhern, T. D.; Bottomley, S. P.; Rossjohn, J. *J. Biol. Chem.* **2004**, *279*, 46448.
(25) Krebs, K. E.; Phillips, M. C. *Biochim. Biophys. Acta* **1983**, 754–227. Eisenberg, D.; Weiss, R. M.; Terwilliger, T. C. *Nature* **1982**, *299*, 371.
(26) Bolanos-Garcia, V. M.; Mas-Oliva, J.; Ramos, S.; Castillo, R. *J. Phys. Chem. B* **1999**, *103*, 6236.
(27) Bolanos-Garcia, V. M.; Ramos, S.; Castillo, R.; Xicohtencatl-Cortes, J.; Mas-Oliva, J. *J. Phys. Chem. B* **2001**, *105*, 5757.
(28) Bolanos-Garcia, V. M.; Nunez-Miguel, R. *Prog. Biophys. Mol. Biol.* **2003**, *83*, 47.
(29) Bolanos-Garcia, V. M.; Renault, A.; Beaufils, S. *Biophys. J.* **2008**, *94*, 1735.
(30) Damodaran, S.; Rao, C. S. *Molecular basis for protein adsorption at fluid-fluid interfaces*; 2001; p 165.
(31) Ward, A. F.; Tordai, L. *J. Chem. Phys.* **1946**, *14*, 453.
(32) Renault, A.; Pezennec, S.; Gauthier, F.; Vie, V.; Desbat, B. *Langmuir* **2002**, *18*, 6887.
(33) Croguennec, T.; Renault, A.; Beaufils, S.; Dubois, J. J.; Pezennec, S. *J. Colloid Interface Sci.* **2007**, *315*, 627.
(34) Gromiha, M. M.; Selvaraj, S. *Prog. Biophys. Mol. Biol.* **2004**, *86*, 235.
(35) Sinclair, C.; Borchers, C.; Parker, C.; Tomer, K.; Charbonneau, H.; Rossie, S. *J. Biol. Chem.* **1999**, *274*, 23666.
(36) Bolanos-Garcia, V. M. *Comput. Biol. Chem.* **2008**, *32*, 139.

JP711222S